Pramana – J. Phys. (2016) 87: 33
DOI 10.1007/s12043-016-1223-9

L subshell fluorescent X-ray measurements to study CK transitions in the $66 \leq Z \leq 83$ region

GURPREET KAUR[1], HIMANI BANSAL[1], M K TIWARI[2] and RAJ MITTAL[1,*]

[1]Nuclear Science Laboratories, Physics Department, Punjabi University, Patiala 147 002, India
[2]X-ray Optics Section, Indus Synchrotron Utilization Division, Raja Ramanna Centre for Advanced Technology, Indore 452 013, India
*Corresponding author. E-mail: rmsingla@yahoo.com

MS received 5 June 2015; revised 2 September 2015; accepted 1 October 2015; published online 27 July 2016

Abstract. L subshell fluorescent X-rays in Dy, Ho, Er, Lu, Ta, W, Pt, Au, Hg, Pb and Bi have been measured using synchrotron with selective creation of electron vacancies in individual subshells. Coster–Kronig (CK) yields were derived from the measured intensities. Present measurements have been made at photon energies above the edges where differences between measured and theoretical attenuation coefficients are almost negligible. Parametric trends for the results with Z were developed to cover all Zs in the range of 66–83. The trends predict the switching-off of L1–L2, N_1 transition at $Z = 67$. The extent of fall/rise of f_{Lij} values corresponding to off/on of certain transitions is found inversely proportional to the difference in binding energies of two consecutive subshells involved in the transition. For Zs above/below these rises/falls, f_{L13} and f_{L12} values are almost constants. f_{L23} values involving no break at Zs follow the general photoionization behaviour that ionization probability is highest at the edge energy and decreases with photon energy. Yield measurements with synchrotron radiation for Dy, Ho, Lu, Hg and Bi and experimental values for f_{L23}, f_{L12} in Lu and for f_{L13} in Ta are being quoted for the first time.

Keywords. L subshell fluorescent X-rays; selective excitation; Coster–Kronig yields; synchrotron photon source; photoionization cross-section.

PACS Nos 32.80.−t; 41.60.Ap; 33.50.−j

1. Introduction

Vacancy created in one of the lower subshells of a shell by primary ionization shifts to a higher subshell due to faster intrashell non-radiative Coster–Kronig (CK) transition in the time interval of the order of 10^{-17} s before an outer shell electron jumps to fill it. CK transition probability f_{Lij} is the probability of shift of the ith subshell vacancy to the jth subshell of L shell. Thus, CK transitions alter the primary vacancy distribution in the shell before filling of vacancies. Vacancies in more tightly bound L1 subshell may shift to L2 or L3 subshell and from L2 subshell to L3 subshell. The probability of a CK transition depends upon the chances of outer shell electron knock out by the energy difference of two subshells i and j of L shell. Therefore, in contrast to other fundamental atomic parameters related to fluorescence processes, those exhibit almost regular variation with atomic number Z, Coster–Kronig transition probabilities display abrupt discontinuities at certain Zs [1] due to switching-on/off of certain outer shell electron knockouts with threshold CK transition energies [2]. Thus, study of CK transitions becomes considerably interesting for checking the configuration of outer shell electrons and the influence of external environment on these electron bindings.

Literature was explored for the existing experimental and theoretical values on L shell CKs. Different groups have measured L shell CK yields for medium and high Z elements employing different experimental methods based on coincidence technique and selective excitation techniques with radioactive sources/X-ray tubes in double reflection geometry or tunable synchrotron radiation sources.

Coincidence technique is appropriate to determine the yields for L2 and L3 subshells as in K–L coincidence pattern emission of $K_{\alpha 1}$ and $K_{\alpha 2}$ characteristic

X-rays leads to primary vacancy distribution in L2 and L3 subshells and emission of L X-rays leads to final vacancy distribution in L2 and L3 subshells, i.e., primary vacancies in L2 and L3 subshells plus vacancies shifted from L2 to L3. Different researchers [3–16] have measured CK yields in rare-earth and high Z elements using radioactive isotopes or photon-induced K–L coincidences.

Selective excitation technique is the production of a vacancy in the specific subshell of a shell, generally, implemented either in double reflection geometry employing radioactive/X-ray tube photon source or with tunable synchrotron photons. It is based on photoionization where reliable values of ionization cross-sections from theoretical calculations or from experimental determinations provide a calibration system with prior knowledge of primary vacancy distribution in individual subshells. Thus, it becomes the most convenient technique for CK measurements.

Since 1976, different researchers [17–24] used double reflection geometries, mostly with ^{241}Am radioactive source, for selective excitation in f_{Lij} measurements. Gupta *et al* [25] measured f_{L23} for W, Pt, Pb and U using triaxial double reflection geometry with X-ray tube source. Radioactive/X-ray tube sources could be used in limited cases depending on the availability of incident photons as particular nuclear decay energies and, in turn, K X-ray energies of primary targets for selective L subshell excitations in the elements under investigation. In all these measurements, interpolated values of photoionization cross-sections from the tables of Scofield [26] were used.

Tunable synchrotron photon beam is ideal for selective photoionization of L subshells. Employing the synchrotron photoionization method, Jitschin *et al* [27] measured f_{L23}, f_{L12} and f_{L13} CK yields for Au using a thin sandwich sample (0.25 pm Cu, 0.2 pm Au, 16 pm Al), whereas the Cu foil was used for normalization. Werner and Jitschin [28] measured the same for elements, with atomic numbers $72 \leq Z \leq 82$, using a thin sandwich sample for normalization in a small vacuum chamber. Sanchez *et al* [29] measured CK yield of Yb and Ta using pure-element foils in synchrotron vacuum chamber. Barrea *et al* [30] measured CK yield of a thick foil of pure Er in vacuum chamber. Kolbe *et al* [31] determined CK transition probabilities of Au, Pb, Mo and Pd using in-house developed ultrahigh vacuum chamber placed in the focal plane of the synchrotron radiation beam lines. Jitschin *et al* [27], Werner and Jitschin [28] and Kolbe *et al* [31] used experimentally determined and Sanchez *et al* [29] and Barrea *et al* [30] used theoretical photoelectric cross-section values for subshells at incident photon energies for CK evaluations. The experimental cross-sections determined were from measured attenuation coefficients after subtracting the coherent and incoherent scattering contributions.

Many relativistic/non-relativistic theoretical, fitted/interpolated and semiempirical values for CK yields are also available in literature. Bambynek *et al* [2] gave theoretical formulation to calculate L shell yields. Krause [32] compiled the fitted values of f_{Lij} for the elements in the range $12 \leq Z \leq 110$. Chen *et al* [33] gave parameter values based on relativistic Dirac–Hartree–Slater (RDHS) model for 25 elements in the range $18 \leq Z \leq 100$. RDHS is a relativistic Dirac approach for atomic structure evaluations for multielectron system using single determinant Slater's approximation for Hartree's self-consistently computed all electron wavefunctions (*Atomic Inner Shell Physics* by B Crasemann, 1985, DOI: 10.1007/978-1-4613-2417-1). Puri *et al* [34] used logarithmic interpolation on CK data of Chen *et al* [33] thereby provided a complete set of RDHS model-based CK yields for $25 \leq Z \leq 96$. Oz *et al* [20] gave semiempirical values of f_{L12} and f_{L23} from fit to measured values with polynomials in Z. McGuire [35] tabulated L shell CK yields for some elements in the atomic range $13 \leq Z \leq 90$ using non-relativistic calculations.

In 2003, Campbell provided a complete compilation of measured values of L shell CK yields and quoted large uncertainties (40–50% in f_{L12}, 10–15% in f_{L13} and 10% in f_{L23}) in the range $71 \leq Z \leq 83$. In 2009, he re-assessed the data on fluorescence and CK yields for L1 subshell in light of the new experimental data [36] and excluding the values of Sogut [22] and McGuire [35], the uncertainties given were 20–40% in f_{L12}, 15–20% in f_{L13}.

In 2012, from the critical analysis of the experimental L shell CK yields from coincidence technique and synchrotron ionization methods, Papp [37] pointed out the need for the measurement of CK parameters as true photoionization cross-sections and true physical parameters.

Present review of theoretical/semiempirical and experimental L shell CK yields allocates percentage differences in available theoretical values of up to 20% in f_{L23}, 69% in f_{L12} and 33% in f_{L13} but differences are high, up to 141% in the comparison of theoretical and semiempirical values. Similarly, the percentage differences in theoretical and experimental values of f_{L23} are up to 48%, 196% in f_{L12} and 23% in f_{L13}. The

differences among the available experimental L shell CK yields using synchrotron radiation is found to be 0–38% and the same between the synchrotron and other experimental methods for almost all cases is up to 62% and higher (191–742%) in some cases.

So, the exploration of L CKs in the region $65 \leq Z \leq 85$ concludes in a vast scattered data with frequent and sharp variations of f_{L13} and f_{L12} predicted by the theory. No single group's extensive measurements are available in the region to support the theory and to certify the facts. Therefore, L CK measurements on the available eleven elements in the range $66 \leq Z \leq 83$ were undertaken in a single experiment.

Keeping in mind the Papp's [37] suggestions, L subshell measurements in the region $66 \leq Z \leq 83$ have been attempted with synchrotron photons at selected incident excitation energies, ∼100–1700 eV away from the edges where the disparity in measured and theoretical extrapolated attenuation coefficients is the least/nil [38]. Thus, the experimentally tested Scofield's [26] photoionization cross-section values were used for CK parameter evaluations. Moreover, the formulation developed for CK parameters is free from the unknown set-up parameters such as source strength, solid angle and detector efficiency. The relations involve only the ratio of quantities; counts under the required X-ray photopeaks, photoionization cross-sections and target self-absorption correction factors at two selective photon energies. Moreover, the ratio of quantities involved in the formulation nullifies systematic errors.

2. Experimental set-up and measurements

Experimental set-up at RRCAT, Indore, India on Microprobe-XRF beam line (BL-16), Indus-II synchrotron source [39,40] was used for the measurements on Dy, Ho, Er, Lu, Ta, W, Pt, Au, Hg, Pb and Bi. The entire experimental station was housed in a large radiation shielded hutch. The geometrical set-up in the hutch comprises the sample positioned at 45° to the incident beam in the horizontal deviation geometry. Fluorescent radiation was detected at 90° with respect to the incident beam with a Peltier-cooled vortex solid-state detector (SII Nano, USA), having an energy resolution of ∼138 eV at 5.959 keV X-rays. The detector was at a distance of ∼30 mm from the sample position. To confine the beam size, a 200 micron slit was inserted in path of the beam to the target (figure 1).

In synchrotron, generally, normalization of the fluorescence intensity is done by recording simultaneously the K fluorescence of a properly chosen element. Jitschin *et al* [41] used gaseous sample for which a chamber was evacuated and then filled with 20 mbar Ar, and finally 20 mbar Xe leading to constant amount of gas during measurement. In the present work, counts under the atmospheric argon (Ar) K X-ray peak were collected in the same spectra and used as a tool to find I_0 (source strength) and normalization.

Experimental targets of Ta, W, Pt, Au, Pb were in metallic form, Ho from Ho_2O_3 powder mixed with borax, while that of Dy, Er, Hg and Bi were self-supporting targets from powders of Dy_2O_3, Er_2O_3, $LuCl_3$, Hg_2Cl_2 and $Bi_2(SO_4)_3$ and styrol [42].

The energies of synchrotron radiation E_3, E_2 and E_1 were picked up to create electron vacancies in selected subshells; only L3, L3 and L2 and all L3, L2 and L1 respectively. The energies along with E_{L3}, E_{L2} and E_{L1} edge energies for target elements are listed in table 1.

Due to the limited resolution of the detector, L lines were grouped in peaks L1, Lα, Lβ, Lγ. Peaks L1 and Lα comprise only L lines feeding the L3 vacancies. Due to the higher intensity of Lα peak to L1, only Lα group comprising the lines L3–M4,5 was involved in the evaluations of f_{L23} and f_{L13}. Lγ peak comprises

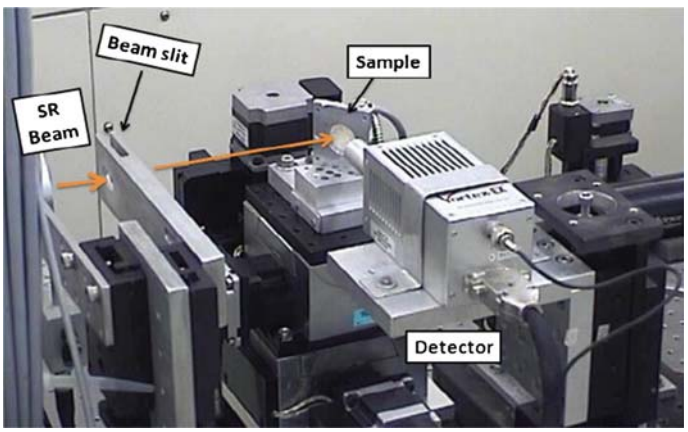

Figure 1. Photograph of the experimental set-up.

Table 1. Excitation energies E_3, E_2 and E_1 and edge energies E_{L3}, E_{L2} and E_{L1} in keV to excite only L3, L3 and L2 and all L3, L2 and L1 subshells.

Z	Experimental targets	E_{L3}	E_3	E_{L2}	E_2	E_{L1}	E_1
66	Dy	7.79	8.00	8.58	9.00	9.05	10.00
67	Ho	8.07	8.50	8.92	9.00	9.39	10.00
68	Er	8.36	9.00	9.26	9.50	9.75	10.00
71	Lu	9.25	10.00	10.35	10.50	10.87	11.00
73	Ta	9.88	10.00	11.14	11.50	11.68	12.00
74	W	10.20	11.00	11.54	12.00	12.10	13.00
78	Pt	11.56	12.00	13.27	13.50	13.88	14.00
79	Au	11.92	13.00	13.73	14.00	14.35	15.00
80	Hg	12.28	14.00	14.21	14.50	14.84	15.00
82	Pb	13.04	14.00	15.20	15.50	15.86	16.00
83	Bi	13.42	14.00	15.71	16.00	16.39	17.00

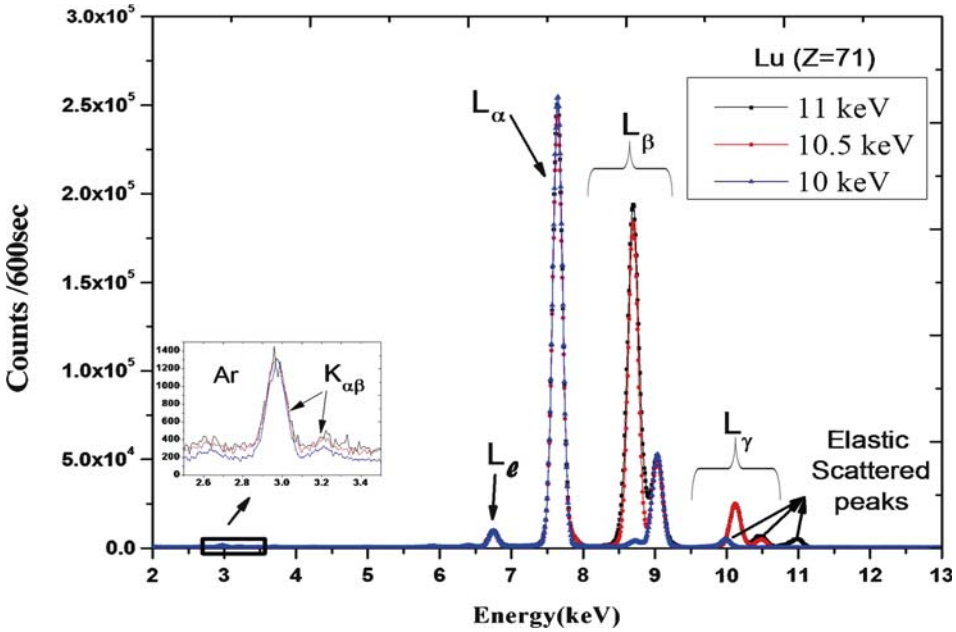

Figure 2. Typical normalized L X-ray spectra of Lu recorded at 10, 10.5 and 11 keV synchrotron photon energies.

the lines feeding the vacancies in L1 and L2 levels only. Therefore, $L_{\gamma 1,5}$ that consists of lines L2–$N_{1,4}$ was used in f_{L12} evaluation. The average X-ray energies $E_{L\alpha}$ and $E_{L\gamma 1,5}$ were calculated using line energies from tables of Storm and Israel [43] weighted with relative intensities [44]. For each experimental target, two spectra were recorded for sufficient counts under the Ar K X-rays with 2% counting statistics. Typical spectra of Lu after normalization with Ar counts recorded at 10, 10.5 and 11 keV are shown in figure 2. The fitted peaks of L_α (Lu), Lγ1,5 (Lu) and $K_{\alpha\beta}$ (Ar) at 11 keV using Gaussian fitting software ORIGIN PRO 8.5 are shown in figure 3.

3. Formulation and calculations

In geometrical arrangement, incident photons of energies E_1, E_2 and E_3, in turn, strike the target at an angle 45° and the emitted fluorescent X-rays are detected at an angle 45° normal to the target. Fluorescent X-ray counts, $N_{L_\alpha/\gamma 1,5}$ and $N_{K_{Ar}}$ at three energies are given as

$$N_{L\alpha}(E_1) = I_0(E_1)\frac{A_v}{M_L}t\beta_{L\alpha}(E_1) \times[\sigma_{L3}(E_1) + \sigma_{L2}(E_1)f_{L23} + \sigma_{L1}(E_1)(f_{L13} + f_{L12}f_{L23})] \times\omega_{L3}F_{L3\alpha}\varepsilon_{L\alpha}, \quad (1)$$

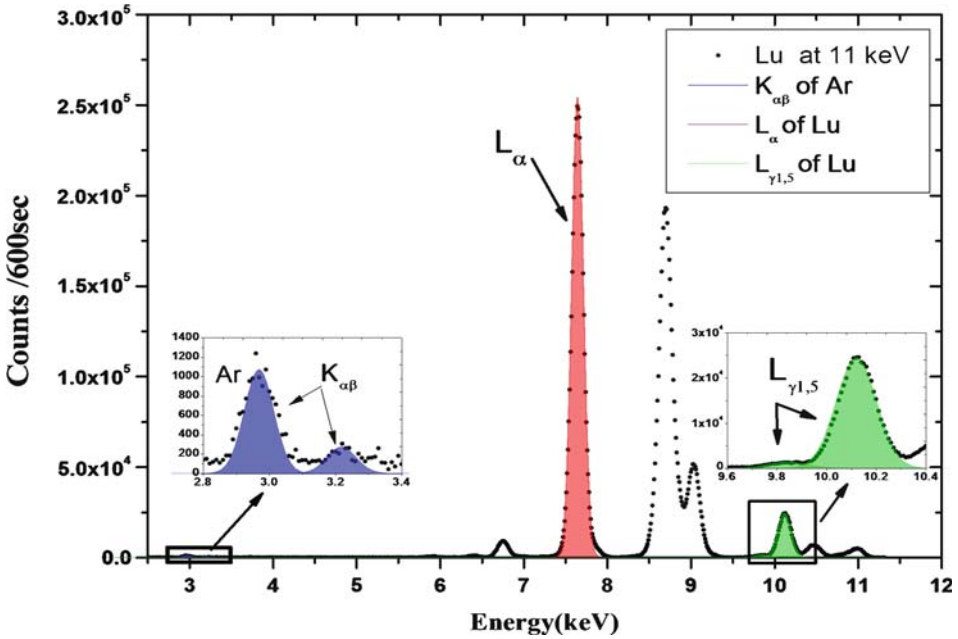

Figure 3. Fitted peaks $K_{\alpha\beta}$ of Ar and $L\alpha$, $L\gamma1,5$ of Lu in the spectrum recorded at 11 keV.

$$N_{L\alpha}(E_2) = I_0(E_2)\frac{A_v}{M_L}t\beta_{L\alpha}(E_2) \times(\sigma_{L3}(E_2)+\sigma_{L2}(E_2)f_{L23}) \times\omega_{L3}F_{L3\alpha}\varepsilon_{L\alpha}, \quad (2)$$

$$N_{L\alpha}(E_3)=I_0(E_3)\frac{A_v}{M_L}t\beta_{L\alpha}(E_3)(\sigma_{L3}(E_3))\omega_{L3}F_{L3\alpha}\varepsilon_{L\alpha}, \quad (3)$$

$$N_{L_{\gamma1,5}}(E_1) = I_0(E_1)\frac{A_v}{M_L}t\beta_{L_{\gamma1,5}}(E_1) \times(\sigma_{L2}(E_1)+\sigma_{L1}(E_1)f_{L12}) \times\omega_{L2}F_{L2\gamma_{1,5}}\varepsilon_{L\gamma1,5}, \quad (4)$$

$$N_{L_{\gamma1,5}}(E_2) = I_0(E_2)\frac{A_v}{M_L}t\beta_{L_{\gamma1,5}}(E_2)\,(\sigma_{L2}(E_2)) \times\omega_{L2}F_{L2\gamma_{1,5}}\varepsilon_{L\gamma1,5}, \quad (5)$$

$$N_{K_{Ar}}(E_1/E_2/E_3) = I_0(E_1/E_2/E_3)\frac{A_v}{M_{Ar}} \times t\beta_{K_{Ar}}(E_1/E_2/E_3) \times\sigma_{K_{Ar}}(E_1/E_2/E_3)\omega_K\varepsilon_K, \quad (6)$$

where $N_{L\alpha}$ and $N_{L\gamma1,5}$ are the counts under the L_α and $L_{\gamma1,5}$ peak respectively of experimental targets at incident energies E_is; $N_{K_{Ar}}$ are the counts under the argon (Ar) K X-ray peak; A_v is the Avogadro's number; M_L is the atomic/molecular weight of the sample target in g; t is the sample thickness in g/cm^2; βs are target self-absorption correction factors at incident and emitted energies; σs are photoionization cross-sections in b/atom; ωs are the fluorescent yield; Fs are the fractional radiative decay rates and ε is the efficiency of the detector at the emitted X-ray energy. $I_0(E_i)$ is the intensity of synchrotron photons at energy E_i striking the target area seen by the detector. In the span of measurements, $I_0(E_i)$ is diminishing, thus, counts under the argon (Ar) K X-ray peak have been used as a tool to find I_0 (source strength).

On solving eqs (2) and (3), (4) and (5), (1) and (3), the relations for CK yield f_{L23}, f_{L12} and f_{L13} respectively were found to be

$$f_{L23} = \left[\frac{N_{L\alpha}(E_2)}{N_{L\alpha}(E_3)}\times\frac{I_0(E_3)}{I_0(E_2)}\times\frac{\beta_{L\alpha}(E_3)}{\beta_{L\alpha}(E_2)} \times\frac{\sigma_{L3}(E_3)}{\sigma_{L3}(E_2)}-1\right]\times\frac{\sigma_{L3}(E_2)}{\sigma_{L2}(E_2)}, \quad (7)$$

$$f_{L12} = \left[\frac{N_{L\gamma1,5}(E_1)}{N_{L\gamma1,5}(E_2)}\times\frac{I_0(E_2)}{I_0(E_1)}\times\frac{\beta_{L\gamma1,5}(E_2)}{\beta_{L\gamma1,5}(E_1)} \times\frac{\sigma_{L2}(E_2)}{\sigma_{L1}(E_1)}\right]-\frac{\sigma_{L2}(E_1)}{\sigma_{L1}(E_1)}, \quad (8)$$

$$f_{L13} = \left[\frac{N_{L\alpha}(E_1)}{N_{L\alpha}(E_3)}\times\frac{I_0(E_3)}{I_0(E_1)}\times\frac{\beta_{L\alpha}(E_3)}{\beta_{L\alpha}(E_1)}\times\frac{\sigma_{L3}(E_3)}{\sigma_{L1}(E_1)} -\frac{\sigma_{L3}(E_1)}{\sigma_{L1}(E_1)}-\left(\frac{\sigma_{L2}(E_1)}{\sigma_{L1}(E_1)}+f_{L12}\right)f_{L23}\right], \quad (9)$$

where

$$\frac{I_0(E_3)}{I_0(E_2)}=\left[\frac{N_{K_{Ar}}(E_3)}{N_{K_{Ar}}(E_2)}\times\frac{\beta_{K_{Ar}}(E_2)}{\beta_{K_{Ar}}(E_3)}\times\frac{\sigma_{K_{Ar}}(E_2)}{\sigma_{K_{Ar}}(E_3)}\right], \quad (10)$$

$$\frac{I_0(E_2)}{I_0(E_1)} = \left[\frac{N_{\mathrm{K_{Ar}}}(E_2)}{N_{\mathrm{K_{Ar}}}(E_1)} \times \frac{\beta_{\mathrm{K_{Ar}}}(E_1)}{\beta_{\mathrm{K_{Ar}}}(E_2)} \times \frac{\sigma_{\mathrm{K_{Ar}}}(E_1)}{\sigma_{\mathrm{K_{Ar}}}(E_2)}\right], \tag{11}$$

$$\frac{I_0(E_3)}{I_0(E_1)} = \left[\frac{N_{\mathrm{K_{Ar}}}(E_3)}{N_{\mathrm{K_{Ar}}}(E_1)} \times \frac{\beta_{\mathrm{K_{Ar}}}(E_1)}{\beta_{\mathrm{K_{Ar}}}(E_3)} \times \frac{\sigma_{\mathrm{K_{Ar}}}(E_1)}{\sigma_{\mathrm{K_{Ar}}}(E_3)}\right]. \tag{12}$$

In CK evaluations, σs were taken from the experimentally tested tables of Scofield [26]; βs [45] were calculated using μs, the absorption coefficient from XCOM [46]. The CK values determined along with available data are listed in table 2.

4. Results and discussions

The methodology followed here for the determination of CK yield is very simple and involves relations (7)–(12). Only σ and β factors are required for $f_{\mathrm{L}ij}$ evaluations in addition to $N_{\mathrm{L}\alpha}$, $N_{\mathrm{L}_{\gamma 1,5}}$, $N_{\mathrm{K_{Ar}}}$ counts under L_α, $\mathrm{L}_{\gamma 1,5}$ and argon (Ar) K X-ray peaks, respectively. The determined CK values involve uncertainties accumulated from 2% of Ar K X-ray/<0.1% of target L X-ray peak areas, neglecting uncertainties in used data values of σs and βs. This results in 30% uncertainties as the expressions (7)–(9) involve the differences in two large terms. Comparison with literature values yields:

(1) Extremely good agreement of $\mathrm{f_{L23}}$ with theoretical/fitted value that lends support to the present measurements and represents the trustworthiness of the results, but for earlier experimental data, deviations are almost $\leq$13%.
(2) f_{L12} values in some rare cases show higher deviations up to 56% when compared with data of other workers and exceptionally 97% from those of Kolbe *et al* [31]. On theoretical/fitted data side, results are more deviated from that of Krause [32] and Oz *et al* [20] results but are close to Chen *et al* [33], Puri *et al* [34] and Campbell [1,36].
(3) Results for f_{L13} are well in agreement with the theoretical and experimental literature values.

The present higher deviations are mostly from Krause's and Oz *et al*'s fitted data values. In case of measurements with synchrotron method [27–31], there is no reliable justification for 153% deviation of f_{L12} value from that of Kolbe *et al* [31] data. The listed value of 0.010±0.009 in table 2 of [31] for f_{L12} in Pb seems to be a typographical error that is too low as compared to other data. Moreover, there is no justification in the paper for such a low value. The agreement of the present results with those from synchrotron measurements of other researcher justifies the use of Scofield's theoretical photoionization cross-section values at excitation energies away from the edges. Moreover, the results from synchrotron measurements are more justified as compared to those from double reflection geometries using radioactive sources, where incident primary K X-rays have energy spread due to the culmination of different X-ray lines under the photopeaks, while synchrotron photons are of single energy. Thus, present investigations clear the ambiguity between the measurements with synchrotron radiation and with some other technique.

L subshell CK yields ($f_{\mathrm{L}ij}$s) in Dy, Ho, Lu, Hg and Bi are measured for the first time using synchrotron radiation. The experimental data values on f_{L23}, f_{L12} in Lu and on f_{L13} in Ta are new additions to the existing data.

Present investigations cover 11 elements out of 18 in the Z range 66–83. To generate data for all the 18 elements, results were used to predict parametric trend for L-shell CK parameters with Z on the lines used earlier for M-shell theoretical data, on average fluorescence yield [45].

The polynomials in Z were fitted to each CK parameter values with the computer software already developed by Mittal *et al* [47]. The trials which produced closest agreement with the actual values were considered. For different CK yields the resulting trials are summarized as

$$\ln\left(f_{\mathrm{L}ij}\right) = \sum_{n=-2}^{n=+1\text{ or}+2} a_n (Z)^n,$$

where n is the power of Z that varies from -2 to $+1$ for f_{L12} and f_{L13} parameter fits and -2 to $+2$ for f_{L23} fit and a_ns are coefficients of fit for the nth power of Z. For each fit, the data values were more than the number of coefficients in the relation, ensuring the optimization of parameters. The uniqueness of the relation was justified with the f_{L23} values, where 11 values were grouped in sets of 5–6 values under different permutations and combinations. For each combination, the same closeness of fitted values with the actual ones represented the uniqueness of the relation. Due to the predicted sudden change at Z=74 [47] in f_{L12} and f_{L13} data because of L1–L2, $\mathrm{N_{1,2\&3}}$ transition offset and L1–L3, $\mathrm{M_{4,5}}$ transition onset [2], Z region 66–83 has been split into two regions 66–74 and 74–83 for the fits to achieve minimum deviations in fitted and exact values. The actual and fitted values are listed in table 3 and coefficients of fit along with percentage deviations of fitted values from the actual ones are listed in table 4.

Table 2. Measured and the available CK yield values for $66 \leq Z \leq 83$.

Z	Present experiment			Earlier theoretical values			Earlier experimental values					
							Synchrotron			Other techniques		
	f_{L23}	f_{L12}	f_{L13}	f_{L23}	f_{L12}	f_{L13}	f_{L23}	f_{L12}	f_{L13}	f_{L23}	f_{L12}	f_{L13}
^{66}Dy	0.142±0.042	0.207±0.062	0.311±0.092	0.146[a,b] 0.143[c] 0.155[d]	0.190[a,c] 0.194[b] 0.217[d,dd]	0.250[a] 0.300[c] 0.335[d] 0.290[dd]	–	–	–	0.145±0.010[b] 0.168±0.013[n]	0.195±0.012[b]	0.302±0.018[b]
^{67}Ho	0.139±0.042	0.216±0.065	0.306±0.092	0.144[a] 0.145[b] 0.142[c] 0.153[d] 0.138[e]	0.190[a,c] 0.193[b] 0.219[d,dd] 0.202[e] 0.218[f]	0.250[a] 0.300[c] 0.338[d] 0.309[e] 0.336[f] 0.296[dd]	–	–	–	0.142±0.011[b] 0.143±0.010[ff]	0.187±0.013[b] 0.194±0.033[g]	0.314±0.025[b]
^{68}Er	0.134±0.040	0.142±0.043	0.306±0.092	0.143[a,b] 0.140[c,d]	0.125[a] 0.192[b] 0.190[c] 0.182[d,dd]	0.280[a] 0.290[c] 0.334[d] 0.300[e]	0.160±0.005[gg]	0.143± 0.010[gg]	0.277±0.009[gg]	0.141±0.011[b] 0.159±0.012[hh]	0.196±0.034[g]	0.309±0.016[b]
^{71}Lu	0.135±0.040	0.139±0.043	0.316±0.092	0.138[a,b] 0.136[c] 0.143[d]	0.125[a] 0.185[b,d,dd] 0.19[c]	0.320[a] 0.282[c] 0.353[d] 0.317[dd]	–	–	–	–	–	0.338±0.021[ab]
^{73}Ta	0.131±0.039	0.131±0.039	0.323±0.097	0.134[a,c] 0.135[b] 0.139[d]	0.125[a] 0.178[b] 0.180[c] 0.186[d,dd]	0.320[a] 0.280[c] 0.351[d] 0.328[dd]	0.111±0.010[l] 0.161± 0.053[ee]	0.104±0.015[l] 0.168±0.039[ee]	0.339 ±0.020[l] 0.322±0.072[ee]	0.200±0.004[q] 0.150±0.007[r]	0.187±0.034[g]	–
^{74}W	0.131±0.039	0.129±0.039	0.328± 0.097	0.132[a] 0.130[b] 0.133[c] 0.140[d] 0.123[e] 0.139[f]	0.125[a] 0.174[b] 0.180[c] 0.186[d, dd] 0.195[e] 0.185[f]	0.320[a] 0.280[c] 0.352[d] 0.332[e] 0.350[f] 0.333[dd]	0.106±0.010[l]	0.102± 0.015[l]	0.325±0.010[l]	0.139±0.013[b] 0.144±0.017[m] 0.146±0.008[n] 0.125±0.008[s]	0.183±0.013[b] 0.188±0.033[g]	0.288±0.020[b] 0.354±0.024[bb]
^{78}Pt	0.125±0.037	0.053±0.016	0.563±0.169	0.126[a,b] 0.124[c] 0.132[d] 0.131[f]	0.067[a,d] 0.154[b] 0.140[c]	0.560[a] 0.500[c] 0.716[d] 0.545[dd]	0.104±0.020[l]	0.066±0.020[l]	0.562±0.020[l]	0.133±0.016[m] 0.112±0.006[u]	0.076±0.015[g]	0.527± 0.027[h]

Table 2. *(Continued)*

Z	Present experiment			Earlier theoretical values			Earlier experimental values					
							Synchrotron			Other techniques		
	f_{L23}	f_{L12}	f_{L13}	f_{L23}	f_{L12}	f_{L13}	f_{L23}	f_{L12}	f_{L13}	f_{L23}	f_{L12}	f_{L13}
^{79}Au	0.124±0.037	0.050±0.015	0.561±0.168	0.124[b] 0.125[a] 0.122[c] 0.129[d,f] 0.132[e]	0.070[a] 0.148[b] 0.140[c] 0.068[d,ad] 0.083[e] 0.071[f]	0.580[a] 0.533[c] 0.711[d,f] 0.644[e] 0.615[dd]	0.100±0.009[j] 0.180±0.040[k] 0.101±0.010[l]	0.047±0.010[j] 0.064±0.040[k] 0.047±0.020[l]	0.590±0.020[j] 0.524±0.075[k] 0.582±0.010[l]	0.125±0.013[b] 0.112±0.004[o] 0.119±0.003[p]	0.152±0.014[b] 0.073±0.015[g] 0.127±0.006[i]	0.620±0.050[a] 0.542±0.022[b] 0.580±0.030[bb]
^{80}Hg	0.124±0.037	0.051±0.015	0.578±0.173	0.123[a] 0.122[b] 0.120[c] 0.128[d] 0.127[f]	0.070[a] 0.142[b] 0.130[c] 0.069[d,f,dd]	0.600[a] 0.563[c] 0.707[d] 0.705[f] 0.615[dd]	–	–	–	0.122±0.001[o] 0.080±0.002[q] 0.188±0.010[r] 0.128±0.008[s] 0.123±0.012[t] 0.123±0.001[u] 0.190±0.010[v]	0.063± 0.012[g] 0.128±0.007[i]	0.582±0.030[ab]
^{82}Pb	0.115±0.035	0.053±0.016	0.606±0.182	0.119[a,b] 0.116[c] 0.123[d] 0.122[f]	0.130[b] 0.120[c] 0.054[d] 0.061[f] 0.064[a,dd]	0.610[a] 0.580[c] 0.708[d] 0.699[f] 0.620[dd]	0.141±0.040[k] 0.091±0.010[l]	0.010±0.009[k] 0.040±0.015[l]	0.664±0.100[k] 0.661±0.010[l]	0.115±0.002[o,u] 0.105±0.011[t] 0.112±0.002[z] 0.112±0.001[aa] 0.130±0.002[y] 0.136±0.016[m] 0.156±0.010[x] 0.164±0.016[w,r]	0.064±0.013[g] 0.105±0.026[y] 0.154±0.040[w] 0.180±0.020[cc]	0.570±0.030[w] 0.580±0.020[cc] 0.658±0.086[y]
^{83}Bi	0.103±0.031	0.052±0.016	0.603±0.181	0.101[e] 0.113[c] 0.117[a,b] 0.121[d]	0.0549[f] 0.055[d] 0.064[a,dd] 0.069[e] 0.110[c] 0.124[b]	0.580[c] 0.620[a,dd] 0.656[e] 0.700[f] 0.703[d]	–	–	–	0.115±0.010[b] 0.135±0.011[n]	0.071±0.012[g] 0.101±0.010[b]	0.579±0.017[b] 0.620±0.025[h] 0.650±0.05[a]

[a][1]; [b][20]; [c][32]; [d][34]; [e][35]; [f][33]; [g][22]; [h][23]; [i][21]; [j][27]; [k][31]; [l][28]; [m][25]; [n][18]; [o][14]; [p][16]; [q][3]; [r][7]; [s][8]; [t][9]; [u][15]; [v][6]; [w][4]; [x][10]; [y][11]; [z][12]; [aa][13]; [bb][24]; [cc][5]; [dd][36]; [ee][29]; [ff][17]; [gg][30]; [hh][19].

Table 3. The actual experimental and fitted CK values for elements $66 \leq Z \leq 83$.

	f_{L23}		f_{L12}		f_{L13}	
Z	Experimental	Fitted	Experimental	Fitted	Experimental	Fitted
66	0.142±0.042	0.141	0.207±0.062	0.219	0.311±0.093	0.311
67	0.139±0.042	0.139	0.216±0.065	0.183	0.306±0.092	0.307
68	0.134±0.040	0.137	0.142±0.043	0.161	0.306±0.092	0.306
69	–	0.135	–	0.148	–	0.308
70	–	0.133	–	0.140	–	0.311
71	0.135±0.040	0.132	0.139±0.042	0.135	0.316±0.095	0.315
72	–	0.132	–	0.133	–	0.320
73	0.131±0.039	0.131	0.131±0.039	0.131	0.323±0.097	0.324
74	0.131±0.039	0.131	0.129±0.039	0.130	0.328±0.098	0.327
75	–	0.130	–	0.087	–	0.408
76	–	0.130	–	0.067	–	0.474
77	–	0.129	–	0.057	–	0.522
78	0.125±0.037	0.127	0.053±0.016	0.052	0.563±0.169	0.554
79	0.124±0.037	0.125	0.050±0.015	0.051	0.561±0.168	0.572
80	0.124±0.037	0.122	0.051±0.015	0.051	0.578±0.0173	0.581
81	–	0.118	–	0.052	–	0.587
82	0.115±0.035	0.112	0.053±0.016	0.052	0.606±0.182	0.594
83	0.103±0.031	0.105	0.052±0.016	0.052	0.603±0.181	0.609

Table 4. Coefficients of fit from the present CK values for elements $66 \leq Z \leq 83$.

	Z	Fit	Deviation	a_{-2}	a_{-1}	a_0	a_1	a_2
f_{L23}	66–83	-2 to $+2$	<3%	−1972372.00	112772.30	−2412.68	22.84	−0.08
f_{L12}	66–74	-2 to $+1$	<15%	2080000.00	−85500.00	1170.00	−5.34	–
	74–83	-2 to $+1$	<2%	9460000.00	−351000.00	4340.00	−17.90	–
f_{L13}	66–74	-2 to $+1$	0%	605000.00	−25500.00	355.00	−1.65	–
	74–83	-2 to $+1$	<2%	−5050000.00	188000.00	−2330.00	9.64	–

Table 3 provides a view of the current experimental results with 30% uncertainties and their fitted values. Table 4 represents the exactness of the fitted data where deviation from actual data is <3% in all cases except when $Z = 66$, 67 and 68, where it is 15% in f_{L12} values. The large deviations can be assigned to lower energy gap <0.5 keV in L1–L2 levels. Thus, fit coefficient and fitted values can confidently be used in applications on CK parameters.

The parametric results were minutely analysed for their Z variation pattern by comparing their plots with those of Campbell [1] in figures 4–6.

Smooth decrease of f_{L23} with Z has point of inflaction around $Z = 74$, almost similar to the DHS pattern. f_{L12} shows sharp fall at $Z = 67$ and 74 and almost constant pattern in the regions $Z = 69$–74, 78–80 and 82–83. In Campbell's illustration, near Z=80 there is a small fall contrary to the present results that show a small rise. f_{L13} patterns in $Z = 66$–74 and 78–83 regions resemble that of Campbell's [1] illustration but the stagnation at Z =75–77 could not be checked with the current experimental data as it is missing at these elements.

To check the sharp transitions in parameter values at certain Z, Sideways, the knockout probabilities of some nearest outer subshell electrons have been explored at intra sub-shell transition energies E_{L1}–E_{L3}, E_{L1}–E_{L2} and E_{L2}–E_{L3} for different Z using Scofield's [26] level energies. For this, plots of the transition energies in terms of binding energy of knocked electron vs. Z are given in figure 7.

The overall view of the present results and transition energy plots in figure 7 predicts that fall/rise in f_{Lij} values corresponds to off/on of electron knocking probability in the outer subshell. The fall/rise extent is inversely proportional to the gap in the binding energies of two consecutive subshells.

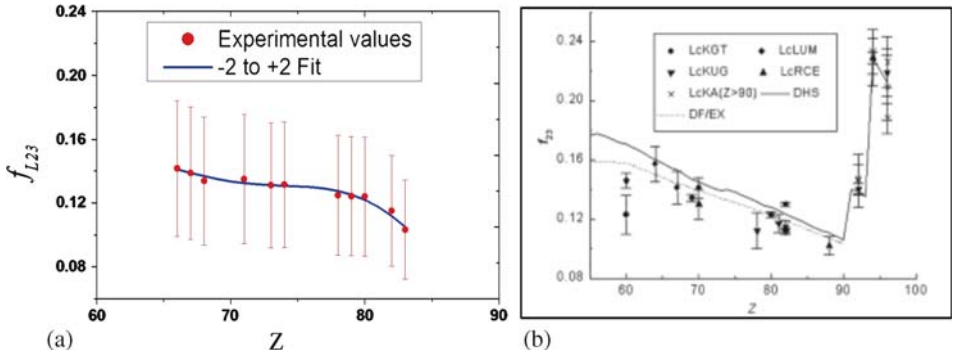

Figure 4. (**a**) Present fitted f_{L23} values vs. atomic number Z and (**b**) Campbell [1] graph for f_{L23} values vs. Z.

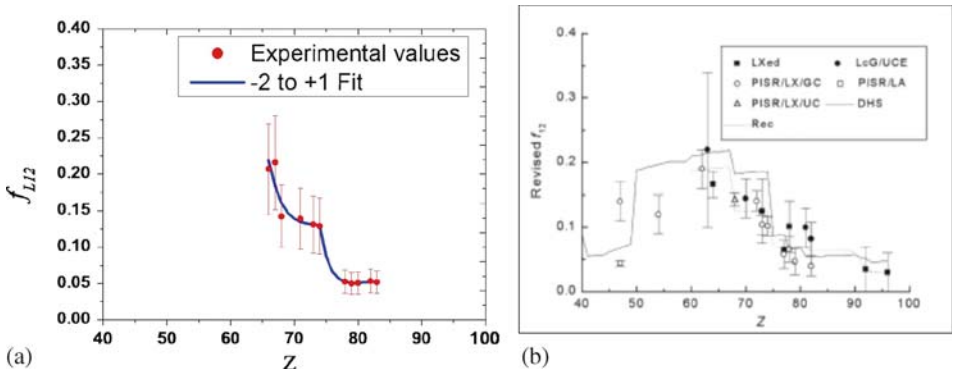

Figure 5. (**a**) Present fitted f_{L12} values vs. atomic number Z and (**b**) Campbell [1] graph for f_{L12} values vs. Z.

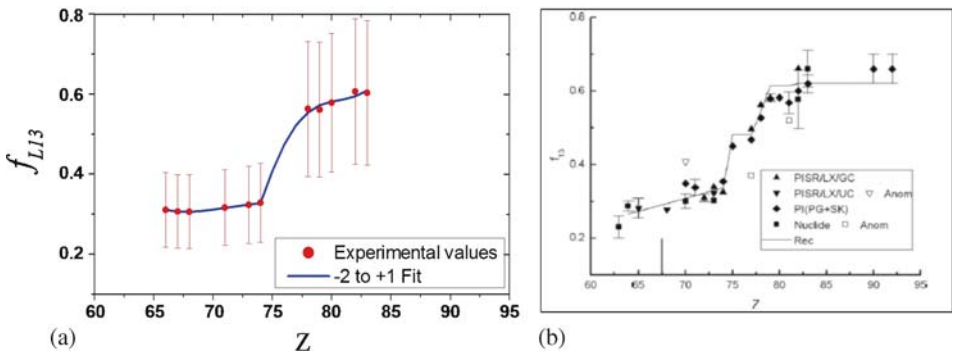

Figure 6. (**a**) Present fitted f_{L13} values vs. atomic number Z and (**b**) Campbell [1] graph for f_{L13} values vs. Z.

(1) In case of f_{L23} there is no on/off of electron knock-out probability in the region $Z = 66$–83 and f_{L23} shows smooth decrease with Z in contrast to the plot of transition energies with Z. It recommends the normal photoionization behaviour that the ionization probability is high for transition energy values nearest to the electron binding energy and the same decreases with increase in transition energy.

(2) Current f_{L12} values have sharp fall at $Z = 67$ and 74 and almost constant values in regions $Z = 68$–74, 78–80 and 82–83 with small rise from 66 to 67 and 80 to 82. This predicts the switching-off of transition L1–L2, N1 at $Z = 67$, though the energy plot represents the switching-off at $Z = 68$. Further, the extent of these rise/fall are found inversely proportional to the binding energy gap between the consecutive outer subshells.

(3) Similarly, in f_{L13} pattern, sudden rise in values at $Z = 68$ and 74 due to the onset of L1–L3, M5 and L1–L3, M4 transitions are inversely proportional to the binding energy gap between the consecutive outer subshells. Again, in regions $Z = 66$–68, 71–74 and 78–83, values are almost constant within experimental errors. All these indicate that under the shadows of sharp rise/fall

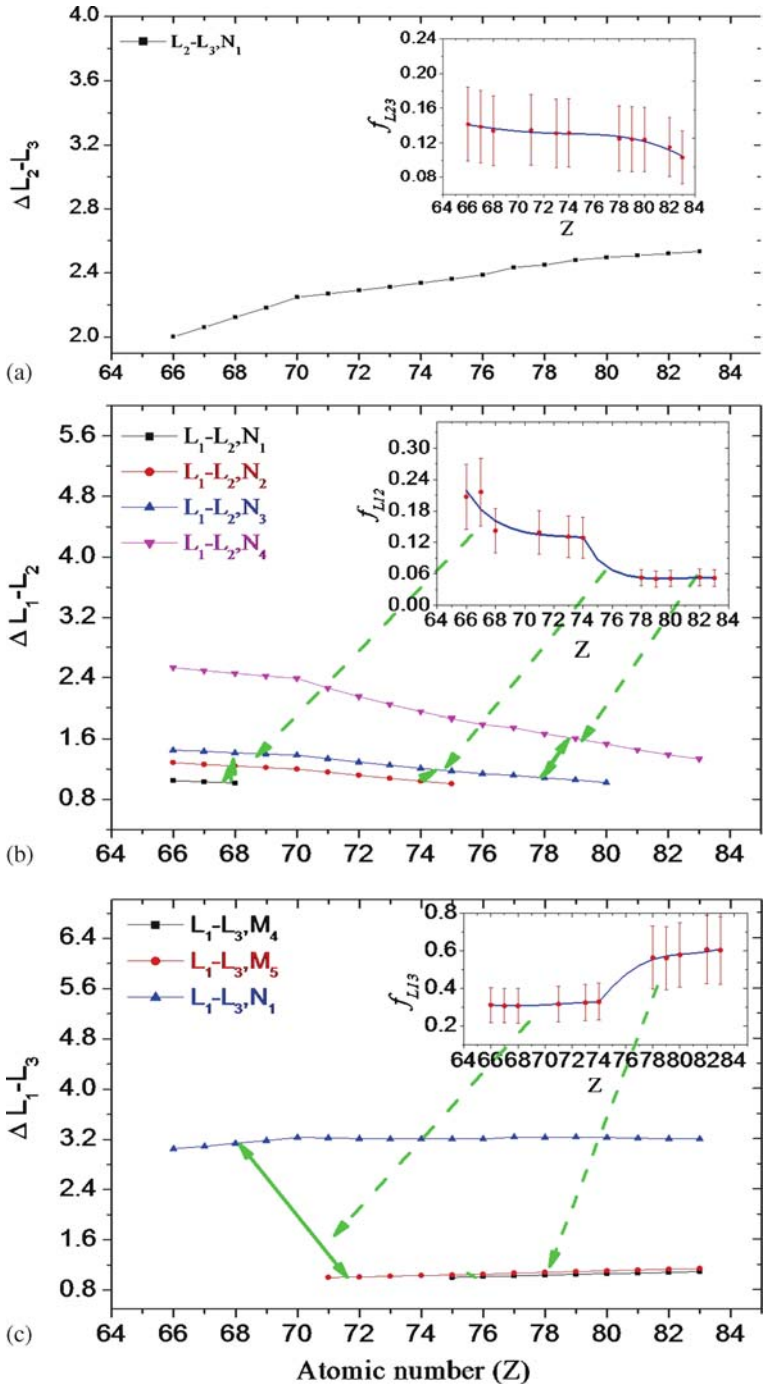

Figure 7. Transition energies (**a**) E_{L2}–E_{L3}, (**b**) E_{L1}–E_{L2} and (**c**) E_{L1}–E_{L3} in terms of binding energies of knocked-out subshell electron (Δ) vs. Z with insets of figures 4a–6a.

in f_{L13} and f_{L12} values, the values in the Z regions in between the rises/falls are almost constants, while f_{L23} involving no break follows the general photoionization behaviour that transition probability is high for transition energies nearest to the knocking electron binding energy and the same decreases with increase in transition energy.

Hence, the present measurements support the theory regarding fall/rise in f_{L13} and f_{L12} values and demonstrate the smooth variation of f_{L23} values with Z (figure 7) as dependence of outer shell electron ionization on incident energy away from the thresholds, i.e., increase in intrashell transition energy with Z results in a decrease in CK f_{L23} values.

5. Conclusions

Yield measurements with synchrotron radiation for Dy, Ho, Lu, Hg and Bi and experimental values for f_{L23}, f_{L12} in Lu and for f_{L13} in Ta are being quoted for the first time. The agreement of the present results with those from synchrotron measurements of other researchers justifies the use of Scofield's theoretical photoionization cross-section values at excitation energies near the edges. Moreover, present investigations clear the ambiguity between the measurements with synchrotron radiation and from some other technique. Parametric trends for the results with Z were developed to cover all Zs in the range of 66–83. The trends predict the switching-off of L1–L2, N1 transition at $Z = 67$. The extent of fall/rise of f_{Lij} values corresponding to off/on of certain transitions is found to be inversely proportional to the difference in binding energies of two consecutive subshells involved in the transition. For Zs above/below these rises/falls, f_{L13} and f_{L12} values are almost constants. f_{L23} values involving no break at Zs follow the general photoionization behaviour that ionization probability is highest at the edge energy and decreases with photon energy.

Acknowledgements

This work is done on Indus-2 synchrotron radiation facility at Raja Ramanna Centre for Advanced Technology, Indore. The accommodating gesture of RRCAT authorities for the experiment, especially the guidance provided by Prof. G S Lodha and financial assistance from UGC-DAE in the form of project grant (CSR-IC-BL-18/CRRS-115/2014-15/1211) are highly acknowledged.

References

[1] J L Campbell, *At. Data Nucl. Data Tables* **85**, 291 (2003)
[2] W Bambynek, B Crasemann, R W Fink, H U Freund, H Mark, C D Swift, R E Prince and P V Rao, *Rev. Mod. Phys.* **44**, 716 (1972)
[3] P V Rao and B Crasemann, *Phys. Rev. A* **139**, 1926 (1965)
[4] P V Rao, R E Wood, J M Palms and W Fink, *Phys. Rev. A* **178**, 1997 (1969)
[5] H U Freud and R W Fink, *Phys. Rev.* **178**, 1952 (1969)
[6] J M Palms, R E Wood, P V Rao and V O Kostroun, *Phys. Rev. C* **2**, 592 (1970)
[7] J C McGeorge, S Mohan and R W Fink, *Phys. Rev. A* **4**, 1317 (1971)
[8] V R Veluri, R E Wood, J M Palms and P V Rao, *J. Phys. B* **7**, 1486 (1974)
[9] D W Nix and R W Fink, *Z. Phys. A* **273**, 305 (1975)
[10] R E Wood, J M Palms and P V Rao, *Phys. Rev. A* **5**, 11 (1972)
[11] M Tan, R A Braga, R W Fink and P V Rao, *Phys. Scr.* **25**, 536 (1982)
[12] J L Campbell, P L McGhee, R R Gingerich, R W Ollerhead and J A Maxwell, *Phys. Rev. A* **30**, 161 (1984)
[13] A L Catz, *Phys. Rev. A* **36**, 3155 (1987)
[14] J L Campbell and P L McGhee, *J. Phys.* **48**, C9-597 (1987)
[15] P L McGhee and J L Campbell, *J. Phys. B* **21**, 2295 (1988)
[16] S Santra, D Mitra, M Sarkar, D Bhattacharya, P Sen and A C Mandal, *Phys. Rev. A* **69**, 024701-1-4 (2004)
[17] D G Douglas, *Can. J. Phys.* **54**, 1124 (1976)
[18] O Simsek, *J. Phys. B* **33**, 3773 (2000)
[19] O Simsek, *Phys. Rev. A* **62**, 052517-1 (2000)
[20] E Oz, N Ekinci, Y Ozdemir, M Ertugrul, Y Sahin and H Erdogan, *J. Phys. B* **34**, 631 (2001)
[21] M Ertugrul, *J. Quant. Spectrosc. Radiat. Transfer* **72**, 567 (2002)
[22] O Sogut, *Instrum. Sci. Technol.* **31**, 85 (2003)
[23] P Singh, A Kumar, D Mehta, K P Singh and N Singh, *Nucl. Instrum. Methods: Phys. Res. B* **196**, 261 (2002)
[24] M Sharma, P Singh, S Puri, D Mehta and N Singh, *Phys. Rev. A* **69**, 032501-1-5 (2004)
[25] S Gupta, V K Mittal and R Mittal, *J. Phys. B* **43**, 235002-1-7 (2010)
[26] J H Scofield, Lawrence Livermore Laboratory, UCRL Report No. 51362 (unpublished) (1973)
[27] W Jitschin, G Materlik, U Werner and P Funke, *J. Phys. B* **18**, 1139 (1985)
[28] U Werner and W Jitschin, *Phys. Rev. A* **38**, 4009 (1988)
[29] H J Sanchez, R D Perez, M Rubio and G Castellano, *Radiat. Phys. Chem.* **48**, 701 (1996)
[30] R A Barrea, C A Perez and H J Sanchez, *J. Phys. B* **35**, 3167 (2002)
[31] M Kolbe, P Honicke, M Muller and B Beckhoff, *Phys. Rev. A* **86**, 042512-1-9 (2012)
[32] M O Krause, *J. Phys. Chem. Ref. Data* **8**, 307 (1979)
[33] M H Chen, B Crasemen and H Mark, *Phys. Rev. A* **24**, 177 (1981)
[34] S Puri, D Mehta, B Chand, N Singh and P N Trehan, *X-ray Spectrom.* **22**, 358 (1993)
[35] E J McGuire, *Phys. Rev. A* **3**, 587 (1971)
[36] J L Campbell, *At. Data Nucl. Data Tables* **95**, 115 (2009)
[37] T Papp, *X-ray Spectrom.* **41**, 128 (2012)
[38] W Jitschin, U Werner, G Materlik and G D Doolen, *Phys. Rev. A* **35**, 5038 (1987)
[39] M K Tiwari, P Gupta, A K Sinha, S R Kane, A K Singh, S R Garg, C K Garg, G S Lodha and S K Deb, *J. Synchrotron. Rad.* **20**, 386 (2013)
[40] G Kaur, S Gupta, M K Tiwari and R Mittal, *Nucl. Instrum. Methods: Phys. Res. B* **320**, 37 (2014)
[41] W Jitschin, R Stotzel, T Papp, M Sarkar and G D Doolen, *Phys. Rev. A* **52**, 977 (1995)
[42] K S Mann, N Singh, R Mittal, K L Allawadhi and B S Sood, *J. Phys. B* **23**, 3521 (1990)
[43] E Storm and H I Israel, *Nucl. Data Tables* **7**, 565 (1970)
[44] S Puri, *At. Data Nucl. Data Tables* **93**, 730 (2007)
[45] G Kaur and R Mittal, *J. Quant. Spectrosc. Radiat. Transfer* **148**, 42 (2014)
[46] M J Berger and J H Hubbell, *XCOM: Photon Cross-sections on a Personal Computer NBSIR 87-3597* (1987)
[47] R Mittal, Vandana and M Singh, *J. Quant. Spectrosc. Radiat. Transfer* **68**, 593 (2001)